

Synthesis, Molecular Properties Prediction and Biological Evaluation of Indole-Vinyl Sulfone Derivatives as Novel Tubulin Polymerization Inhibitors Targeting the Colchicine Binding Site

Wenlong Li^a, Honghao Sun^a, Feijie Xu^a, Wen Shuai^a, Jie Liu^a, Shengtao Xu^{a,*}, Hequan Yao^a, Cong Ma^b, Zheyang Zhu^{c,*}, Jinyi Xu^{a,*}

^aState Key Laboratory of Natural Medicines and Department of Medicinal Chemistry, China Pharmaceutical University, 24 Tong Jia Xiang, Nanjing 210009, P. R. China

^bState Key Laboratory of Chemical Biology and Drug Discovery, and Department of Applied Biology and Chemical Technology, The Hong Kong Polytechnic University, Kowloon, Hong Kong

^cDivision of Molecular Therapeutics & Formulation, School of Pharmacy, The University of Nottingham, University Park Campus, Nottingham NG7 2RD, U. K.

*Corresponding Author:

E-mail addresses: cpuxst@163.com (S. Xu); zheyang.zhu@nottingham.ac.uk (Z. Zhu); jinyixu@china.com (J. Xu).

Abstract

Twenty-two novel indole-vinyl sulfone derivatives were designed, synthesized and evaluated as tubulin polymerization inhibitors. The physicochemical and drug-likeness properties of all target compounds were predicted by Osiris calculations. All compounds were evaluated for their antiproliferative activities, among them, compound **7f** exhibited the most potent activity against a panel of cancer cell lines, which was 2-7 folds more potent than our previously reported compound **4**. Especially, **7f** displayed about 8-fold improvement of selective index as compared with compound **4**, indicating that **7f** might have lower toxicity. Besides, **7f** inhibited the microtubule polymerization by binding to the colchicine site of tubulin. Further

investigations showed that compound **7f** effectively disrupted microtubule network, caused cell cycle arrest at G2/M phase and induced cell apoptosis in K562 cells. Moreover, **7f** reduced the cell migration and disrupted capillary-like tube formation in HUVEC cells. Importantly, the *in vivo* anti-tumor activity of **7f** was validated in H22 liver cancer xenograft mouse model without apparent toxicity, suggesting that **7f** is a promising anti-tubulin agent for cancer therapy.

Key words: tubulin inhibitor; vinyl sulfone; indole; colchicine site; drug-likeness.

1. Introduction

Microtubules are mainly composed of α,β -tubulin heterodimers, and they have several key roles that are crucial for cell proliferation, trafficking, signaling and migration in eukaryotic cells [1-3]. According to the effects on microtubule polymer mass at high concentrations, microtubule targeting agents (MTAs) are classified into two classes: microtubule-stabilizing agents (MSAs) and microtubule-destabilizing agents (MDAs) [4, 5]. MSAs including taxanes and epothilones promote microtubule polymerization, while MDAs inhibit microtubule polymerization and most of these agents bind in either the vinca or the colchicine binding site of tubulin [4]. Inhibitors that target colchicine binding site have advantages over other site binders, such as simpler structures, improved aqueous solubility, reduced toxicity and multidrug resistance (MDR) effects [5-8]. Besides, they can induce the morphological changes in the endothelial cells thus provoking a rapid collapse of the tumor vasculature, which is commonly designated as vascular disrupting activity [9, 10].

Colchicine (**1**) (Fig.1), a representative natural tubulin polymerization inhibitor that target colchicine binding site, was a powerful antimitotic agent to study the tubulin target. It has been used for the treatment of gout, familiar Mediterranean fever, osteoarthritis, pericarditis, and atherosclerosis [11]. Another typical colchicine binding site inhibitor from natural sources is combretastatin A-4 (CA-4, **2**) which was isolated from the bark of the African willow tree *Combretum caffrum*. CA-4 was proved to be a typical tubulin inhibitor binding to the colchicine binding site and

endowed with potent antimitotic and vascular disrupting profiles [12]. However, isomerization of the active *cis*-olefinic conformation into the corresponding inactive *trans*-analogs impeded the clinical development of CA-4 [13], thus hundreds of colchicine binding site inhibitors (CBSIs) have been designed and synthesized mimicking the structure of CA-4 [14-16].

Indole, an important nucleus of many biologically active natural and synthetic products, has been utilized in the construction of CBSIs and was found to be an alternative of 4-methoxyphenyl motif that often occurred in natural CBSIs [17-19]. Our group have been concentrating on discovering and developing novel anti-cancer agents targeting tubulin-microtubule system, such as chalcone analogs bearing vinyl sulfone skeleton [20], 4-arylisochromenes [21] and quinazolines that occupy three zones of colchicine domain [22]. In our previous works on the discovery of analogs of chalcone compound **3** (Fig.2), vinyl sulfone or sulfoxide were incorporated into the structure of **3** to afford a novel series of tubulin polymerization inhibitors [20]. Among them, compound **4** exerted moderate antiproliferative activity with an IC₅₀ value of 0.128 μ M against K562 cell line. However, the unmasked anilide of compound **4** has the potential to form reactive intermediate under metabolic activation process, inducing adverse drug reactions (ADRs) [23]. An example of this is tacrine, which was approved by the US Food and Drug Administration as the first acetylcholinesterase inhibitor for Alzheimer disease treatment [24], however, it has been withdrawn due to its severe hepatotoxicity which might be attributed to the existence of unmasked amino group [25]. With the aims of improving both antiproliferative activity and drug-like property of compound **4** as well as completing the structure activity relationships (SARs) of this novel vinyl sulfone skeleton as anti-tubulin agents, the unmasked amino group was fused with the benzene ring to form indole which is a privileged moiety of CBSIs (Fig.2). Considering the vital effects of the substitution positions of indoles [26, 27], various indoles were firstly incorporated into this new skeleton. Besides, different substituted groups were also introduced to the α position of the sulfones or sulfoxides. All title compounds were then subjected to Osiris calculations to predict their drug-like properties. Herein, we would like to

report their synthesis, molecular properties prediction, *in vitro* and *in vivo* antitumor activities and mechanism studies as novel tubulin polymerization inhibitors targeting the colchicine binding site.

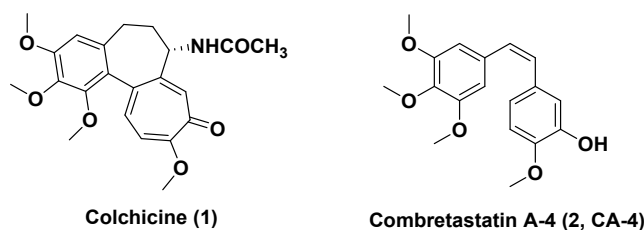


Figure 1. Structures of typically natural colchicine binding site inhibitors

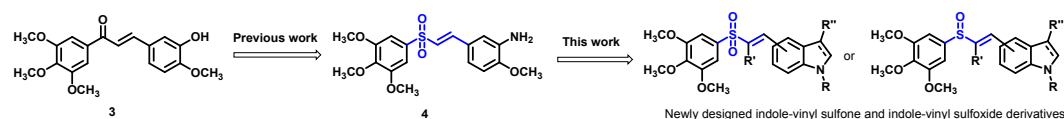


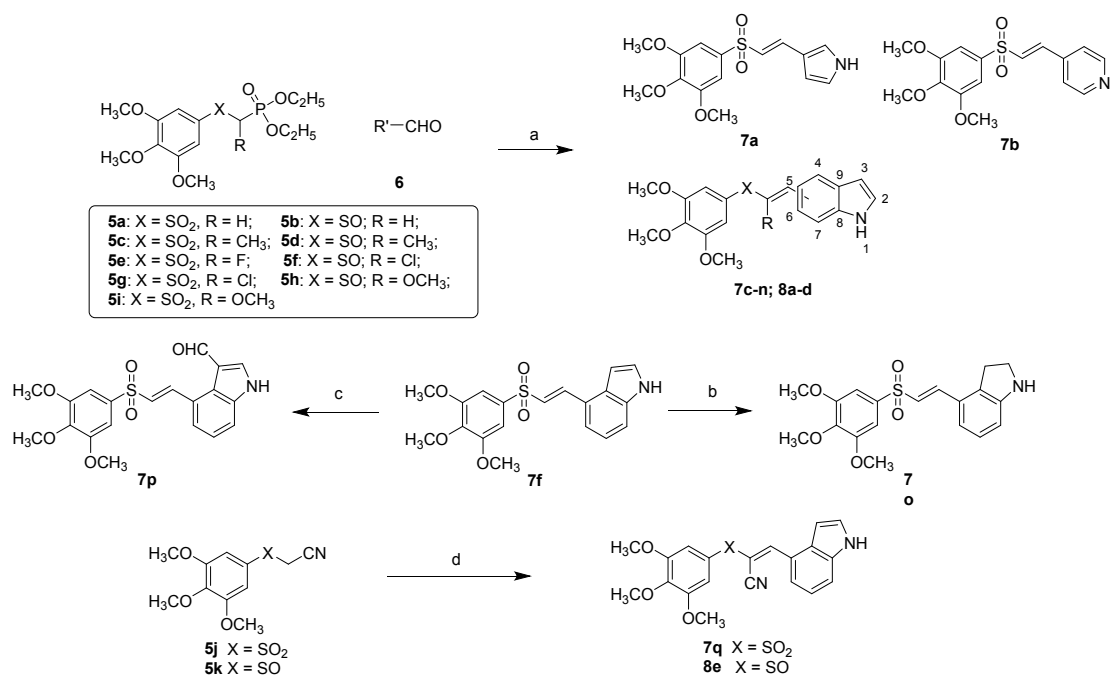
Figure 2. Design strategy of indole-vinyl sulfone or sulfoxide derivatives.

2. Results and discussion

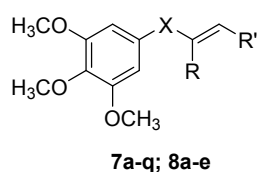
2.1 Chemistry

The synthetic route to indole-sulfone or sulfoxide derivatives is outlined in Scheme 1. The phosphonate intermediates with sulfone or sulfoxide group were prepared according to our previous methods [20]. Various aldehydes were undergone Wittig-Horner reactions with phosphonates **5a-i** to afford the indole-vinyl sulfones **7a-n** and indole-vinyl sulfoxides **8a-d**. The reduction of **7f** in AcOH with NaBH₃CN as the reductant afforded compound **7o**, and **7p** was produced by the Vilsmeier reaction of **7f**. Cyan-substituted indole-vinyl sulfone **7q** and indole-vinyl sulfoxide **8e** were synthesized through Knoevenagel reactions of indole-4-aldehyde with intermediates **5j** and **5k**, respectively. Altogether, twenty-two compounds were finally synthesized as shown in Fig. 3.

Scheme 1. The synthetic route of compounds **7a-q** and **8a-e**.



Reagents and conditions: (a) NaH, THF, N₂, 1 h; (b) NaBH₃CN, AcOH, 1 h; (c) POCl₃, DMF, 30 min; (d) indole-4-aldehyde, piperidine (cat.), AcOH (cat.), toluene, reflux, 2 h.



- 7a** X = SO₂, R = H, R' = 3'-pyrrole;
7b X = SO₂, R = H, R' = 4'-pyridine;
7c X = SO₂, R = H, R' = 3'-(5-Methoxyindole);
7d X = SO₂, R = H, R' = 3'-(6-Methoxyindole);
7e X = SO₂, R = H, R' = 3'-indole;
7f X = SO₂, R = H, R' = 4'-indole;
7g X = SO₂, R = H, R' = 5'-indole;
7h X = SO₂, R = H, R' = 6'-indole;
7i X = SO₂, R = H, R' = 7'-indole;
7j X = SO₂, R = CH₃, R' = 4'-indole;
7k X = SO₂, R = F, R' = 4'-indole;
7l X = SO₂, R = Cl, R' = 4'-indole;
7m X = SO₂, R = OCH₃, R' = 4'-indole;
7n X = SO₂, R = H, R' = 4'-(N-methylindole);
7o X = SO₂, R = H, R' = 4'-(2H-indole);
7p X = SO₂, R = H, R' = 4'-(3-indolealdehyde);
7q X = SO₂, R = CN, R' = 4'-indole;
8a X = SO, R = H, R' = 4'-indole;
8b X = SO, R = CH₃, R' = 4'-indole;
8c X = SO, R = Cl, R' = 4'-indole;
8d X = SO, R = H, R' = 4'-(N-methylindole);
8e X = SO, R = CN, R' = 4'-indole;

Figure 3. The designed indole-vinyl sulfone and indole-vinyl sulfoxide derivatives.




































2.2 Calculation of physicochemical and drug-likeness properties

Drug-likeness can be considered as a delicate balance among the molecular properties of a compound that influences its pharmacodynamics, pharmacokinetics and ultimately ADME (absorption, distribution, metabolism and excretion) in human body like a drug [28-29]. Lipophilicity (logP), solubility (clogS) and topological polar surface area (TPSA) values are important descriptors for charactering physical

properties, permeability, absorption, distribution and bioavailability of the drugs [30-32]. Thus, to evaluate the drug-likeness character of our compounds, toxicity risks (mutagenicity, tumorigenicity, irritation, and reproduction), as well as physicochemical properties (cLogP, cLogS, TPSA), drug likeness and drug score were predicted using Osiris Property explorer [33]. As shown in Table 1, all new designed compounds **7a-q** and **8a-e** were predicted to be without toxicity risks, whereas compound **4** was mutagenic, tumorigenic and irritant, and CA-4 had reproductive effect. All tested compounds were predicted to have good clogP (< 5) and TPSA ($< 140 \text{ \AA}^2$) parameters, and the solubility of compounds **7c-m**, **7o-q**, **8c** and **8e** were in an acceptable range ($\text{clog S} < -4$). As for the drug-likeness and drug score predictions, most of our compounds possessed good drug-likeness scores except compounds **7p**, **7q** and **8e** which bear aldehyde or cyan groups. Our previously reported compound **4** had the lowest drug score probably due to the existence of unmasked amino group. Altogether, these newly designed indole-vinyl sulfone derivatives are supposed to have enhanced physical and drug-likeness properties than compound **4** or CA-4, which prompted us to further evaluate their *in vitro* activities.

Table 1. Osiris calculations of all target compounds **7a-q**, **8a-e**, **4** and CA-4.

Compd.	Toxicity Risks ^a				Physicochemical Parameters and Drug Score					
	MUT	TUM	IRRIT	RE	clogP	clogS	MW	TPSA	drug-likeness	drug score
7a					0.95	-2.79	323.0	86.0	2.04	0.84
7b					1.23	-2.97	335.0	83.1	1.15	0.77
7c					2.2	-4.31	403.0	95.23	0.24	0.56
7d					2.2	-4.31	403.0	95.23	2.9	0.69
7e					2.27	-4.29	373.0	86.0	3.0	0.72
7f					2.27	-4.29	373.0	86.0	1.73	0.68
7g					2.27	-4.29	373.0	86.0	2.11	0.70
7h					2.27	-4.29	373.0	86.0	2.53	0.71
7i					2.27	-4.29	373.0	86.0	2.35	0.71
7j					2.99	-4.67	387.0	86.0	1.88	0.62
7k					2.91	-5.0	391.0	86.0	0.39	0.51
7l					3.55	-4.92	407.0	86.0	1.90	0.45
7m					2.64	-4.54	403.0	95.23	1.62	0.62
7n					2.40	-3.95	387.0	75.14	2.74	0.73
7o					1.90	-4.17	375.0	82.24	2.42	0.72

7p					2.2	-4.61	401.0	103.0	-0.14	0.5
7q					2.24	-4.82	398.0	109.7	-2.04	0.37
8a					2.77	-3.46	357.0	79.76	1.89	0.75
8b					3.5	-3.85	371.0	79.76	2.01	0.69
8c					4.06	-4.09	391.0	79.76	2.05	0.62
8d					2.9	-3.12	371.0	68.9	2.91	0.78
8e					2.74	-4.0	382.0	103.5	-1.90	0.42
4					1.48	-3.86	379.0	105.4	0.69	0.14
CA-4					3.24	-3.53	316.0	57.15	4.56	0.48

^a MUT: mutagenic; TUM: tumorigenic; IRRIT: irritant; RE: reproductive effective, green represents non-toxic and red represents toxic.

2.3 *In vitro* anti-proliferative activity

To identify the best substitution position at indole ring, seven compounds **7c-i** with varying substitution positions at indole ring were firstly screened for their anti-proliferative activities in human leukemia cells (K562) by MTT assays. Another two compounds **7a** and **7b** containing pyrrole and pyridine, respectively, were also investigated. The results in Fig. 4 suggested that compound **7f** with substitution at C-4 position of indole ring exhibited the most potent activity at both 1 μ M and 0.1 μ M concentrations. Other substitution positions on the indole ring led to a significant decrease of activity except compound **7e** which was substituted at C-3 position. Compound **7e** showed potent cytotoxicity with an inhibitory rate of 83.3% at 1 μ M, however, the activity declined dramatically when the concentration decreased to 0.1 μ M. Besides, the placements of ring B with pyrrole (**7a**) and pyridine (**7b**) also led to the loss of activity. Thus, C-4 substituted indole ring was chosen as ring B for next round modification.

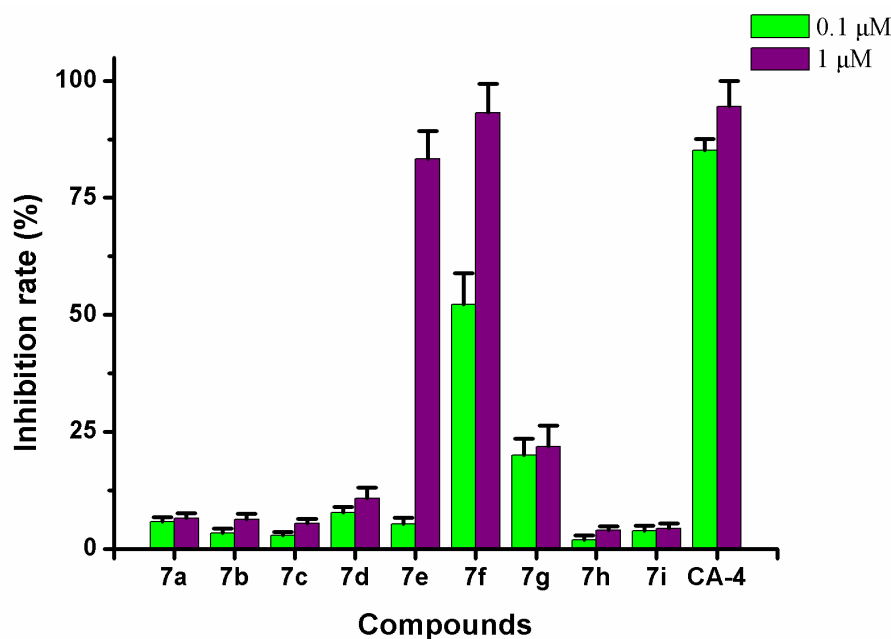


Figure 4. Histograms display the inhibitory rates of compounds **7a-i** against K562 cells.

To investigate the effects of indole ring and substitutions at the α position of sulfone or sulfoxide on the anti-proliferative activity, thirteen compounds **7j-q** and **8a-e** were further synthesized and evaluated against three cancer cell lines including human hepatocellular carcinoma cells (HepG2), human lung adenocarcinoma cells (A549) and human leukemia cell lines (K562) with CA-4 as the positive control. The cytotoxicity data are listed in Table 2, and the results showed that most of the compounds with a C-4 position substituted indole exhibited potent activities against these three cancer cell lines. Among them, vinyl sulfone compound **7f** with R being H was the most active one with an IC_{50} of 55 nM against K562 cell line, which was 2-fold more potent than compound **4**. Besides, the result that R being H was the most appropriate option is in accordance with our previous conclusion that substitutions at the α position of sulfone or sulfoxide would lead to a decrease of cytotoxicity [20]. When R was OCH_3 or CN, compounds **7m**, **7q** and **8e** showed much less potent activity. Furthermore, the reduction of indole to 2H-indole (**7o**) or modified as *N*-methyl indole (**7n** and **8d**) all led to slightly decreased activity while aldehyde group substituted at C-3 position of indole (**7p**) led to a significant loss of activity. Other cell lines including human colon cancer cell (HCT-8), human hepatocellular carcinoma

(Bel-7402), mice hepatocellular carcinoma (H22) and human normal liver cell line (LO2) were chosen for further evaluation of activity of compounds **4** and **7f**. As shown in Table 3, **7f** exhibited 2-7 folds improvement of activity than compound **4** against three cancer cell lines, while **7f** displayed comparable cytotoxicity against LO2 cells to compound **4**. The SI value (selective index, IC_{50} normal cells/ IC_{50} tumor cells) of **7f** was 3.0 which was about 8-fold higher than that of **4**, indicating that **7f** might have lower toxicity.

Table 2 Anti-proliferative activity of compounds against three human cancer cell lines.^a

Compd.	IC_{50} values (μ M) ^b		
	HepG2	A549	K562
7e	0.244±0.012	1.859±0.497	0.323±0.029
7f	0.075±0.005	0.305±0.026	0.055±0.005
7j	0.290±0.008	1.487±0.297	0.774±0.020
7k	0.183±0.021	2.132±0.048	0.110±0.013
7l	0.145±0.004	1.047±0.083	0.220±0.009
7m	>5	>5	>5
7n	0.587±0.046	3.182±0.311	0.891±0.047
7o	0.319±0.010	2.212±0.284	0.305±0.022
7p	>5	>5	>5
7q	>5	>5	>5
8a	0.096±0.012	0.548±0.072	0.141±0.021
8b	0.288±0.042	1.621±0.151	0.275±0.025
8c	0.218±0.029	1.651±0.219	0.307±0.006
8d	0.194±0.031	0.378±0.004	0.294±0.050
8e	>5	>5	>5
4	0.217±0.015	0.606±0.084	0.128±0.003
CA-4	0.012±0.001	0.037±0.001	0.021±0.001

^a Cell lines were treated with different concentrations of compounds for 72 h. Cell viability was measured by MTT assay as described in the Experimental Section.

^b IC_{50} values are indicated as the mean ± SD (standard error) of at least three independent experiments.

Table 3 Anti-proliferative activity of compounds against different cell lines.^a

Compd.	IC_{50} values (μ M) ^b				SI ^c
	HCT-8	H22	Bel-7402	LO2	

4	0.555±0.095	0.105±0.022	0.547±0.097	0.220±0.082	0.4
7f	0.287±0.034	0.060±0.015	0.080±0.023	0.240±0.090	3.0

^a Cell lines were treated with different concentrations of compounds for 72 h. Cell viability was measured by MTT assay as described in the Experimental Section.

^b IC₅₀ values are indicated as the mean ± SD (standard error) of at least three independent experiments.

^c Selectivity index = (IC₅₀ LO2)/(IC₅₀ Bel-7402).

2.4 *In vitro* tubulin polymerization inhibitory assay and colchicine binding assay

Considering the critical roles of microtubules in cell proliferation, trafficking, signaling and migration in eukaryotic cells, we also evaluated the inhibitory efficacy of **7f** that was the most potent compound in cytotoxic assays on microtubule polymerization *in vitro*. The typical microtubule-destabilizing agent colchicine and microtubule-stabilizing agent taxol were employed as the references. As shown in Fig. 5, taxol exhibited a significant promotion of tubulin polymerization, while compound **7f** displayed a concentration dependent inhibition of tubulin polymerization, indicating that the mechanism of **7f** was in accordance with colchicine as a microtubule-destabilizing agent. The calculated IC₅₀ value of **7f** in inhibiting tubulin polymerization was 3.09 μM, which was more potent than compound **4** (IC₅₀ = 4.25 μM) (Table 4). In addition, **7f** competed with [3H]-colchicine in binding to tubulin. The binding potency of **7f** to the colchicine binding site was 69.4% and 84.7% at 1 μM and 5 μM, respectively (Table 4), indicating that **7f** binds to the colchicine binding site. Therefore, taking considerations of the good activities of compound **7f** showing both in the *in vitro* antiproliferative assay and tubulin polymerization inhibition assay, **7f** was selected for further biological studies.

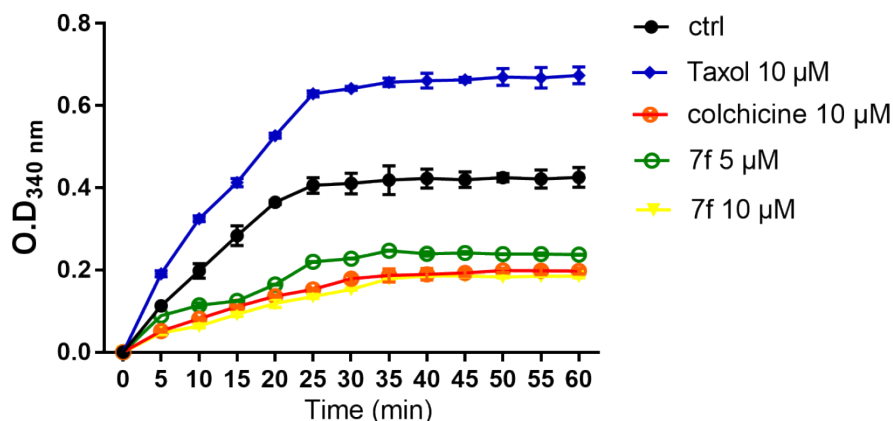


Figure 5. Effect of **7f** on tubulin polymerization *in vitro*. Purified tubulin protein at 2 mg/mL in a reaction buffer was incubated at 37 °C in the presence of 1% DMSO, test compounds (**7f** at 5 or 10 μM), colchicine (10 μM) or Taxol (10 μM). Polymerizations were followed by an increase in fluorescence emission at 350 nm over a 60 min period at 37 °C. The experiments were performed three times.

Table 4. Inhibition of tubulin polymerization^a and colchicine binding to tubulin^b

Compd.	Inhibition of tubulin polymerizaion		Inhibition of colchicine binding (%) inhibition ± SD	
	IC ₅₀ (μM)		1 μM	5 μM
7f	3.09 ± 0.10		69.4 ± 1.9	84.7 ± 3.2
4	4.25 ± 0.75		67.3 ± 2.2	79.8 ± 1.5
CA-4	2.17 ± 0.02		81.2 ± 2.0	91.7 ± 4.4

^a The tubulin assembly assay measured the extent of assembly of 2 mg/mL tubulin after 60 min at 37 °C. Data are presented as mean from three independent experiments.

^b Tubulin, 1 μM; [3H]-colchicine, 5 μM; and inhibitors, 1 or 5 μM.

2.5 Anti-microtubule effects in K562 cells

Since the tubulin polymerization inhibitory effect of **7f** has been verified *in vitro*, we subsequently performed the immunofluorescence assays to investigate the effects of compound **7f** on microtubule networks. As shown in Fig. 6, K562 cells without drug treatment exhibited normal filamentous microtubules arrays. However, after exposure to **7f** at three different concentrations (0.03 μM, 0.06 μM, and 0.12 μM) for 24 h, the microtubule network in cytosol was disrupted, these results indicated that **7f** can induce a dose-dependent collapse of the microtubule network.

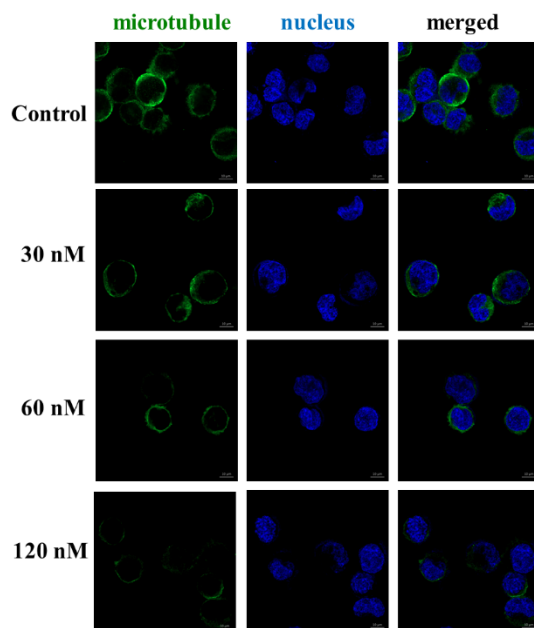


Figure 6. Effects of compound **7f** on the cellular microtubule network visualized by immunofluorescence. K562 cells were treated with vehicle control 0.1% DMSO, **7f** (0.03 μM), **7f** (0.06 μM), **7f** (0.12 μM). Then, the cells were fixed and stained with anti- α -tubulin-FITC antibody (green), and counterstained with DAPI (blue). The detection of the fixed and stained cells was performed with an LSM 570 laser confocal microscope (Carl Zeiss, Germany).

2.6 Cell cycle analysis

Since most microtubule polymerization inhibitors disrupt cell mitosis and exert cell cycle arrest effects, we examined the effect of compound **7f** on cell cycle progression using propidium iodide (PI) staining by flow cytometry analysis in K562 cells. As depicted in Fig. 7A and 7B, compound **7f** caused a concentration-dependent G2/M arrest in K562 cells. When treated with **7f** at 0.03, 0.06, and 0.12 μM for 48 h, the percentages of cells arrested at the G2/M phase were 10.2%, 13.7% and 20.4%, respectively. These results demonstrated that **7f** disrupted the dynamic balance of the tubulin-microtubule system and further induced the cell cycle arrest at the G2/M phase.

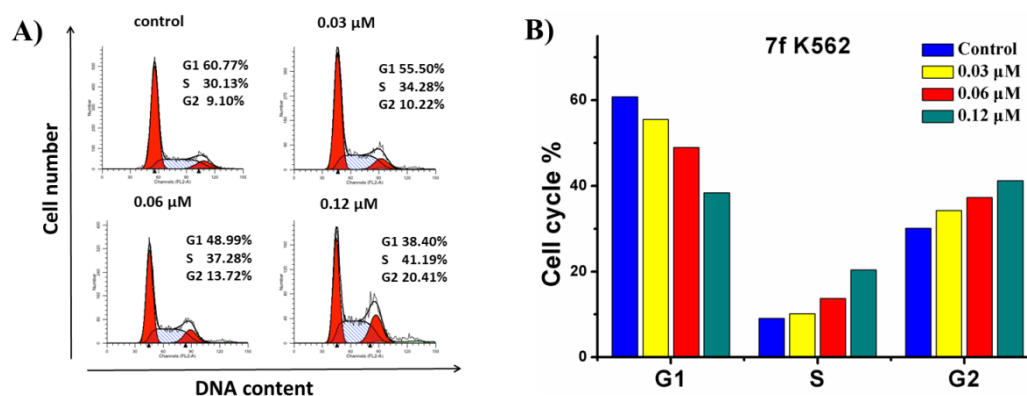


Figure 7. (A) Compound **7f** induced G2/M arrest in K562 cells. K562 cells were incubated with varying concentrations of **7f** (0, 0.03, 0.06, 0.12 μM) for 48 h. Cells were harvested and stained with PI and then analyzed by flow cytometry. The percentages of cells in different phases of cell cycle were analyzed by ModFit 4.1; (B) Histograms display the percentage of cell cycle distribution after treatment with **7f**.

2.7 Cell apoptosis analysis

To assess whether compound **7f** would induce cell apoptosis, an Annexin V-FITC and propidium iodide (PI) assay was carried out. As shown in Fig. 8A and 8B, compound **7f** induced K562 cell apoptosis in a dose-dependent manner. The percentage of apoptotic cells after the 48 h treatment was only 1.46% in the control group. The total numbers of early (Annexin-V⁺/PI⁻) and late (Annexin-V⁺/PI⁺) apoptotic cells increased to 24.8%, 49.3% and 67.6% after treatment with **7f** at 0.03, 0.06, 0.12 μM for 48 h, respectively. These results confirmed that compound **7f** effectively induced cell apoptosis in K562 cells in a dose-dependent manner.

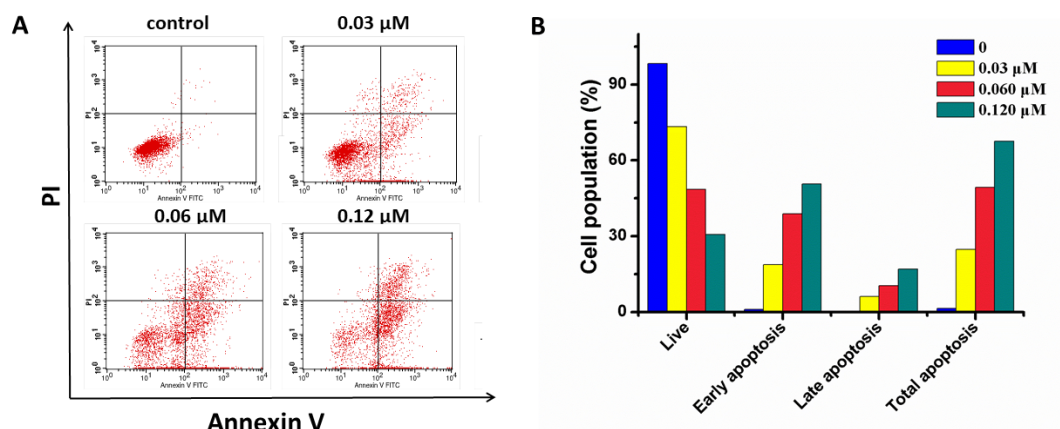


Figure 8. (A) Compound **7f** induced apoptosis in K562 cells. K562 cells were incubated with

varying concentrations of **7f** (0, 0.03, 0.06, and 0.12 μM). After 48 h of incubation, cells were collected and stained with Annexin V/PI, followed by flow cytometric analysis. The percentages of cells in each stage of cell apoptosis were quantified by flow cytometry: (upper left quadrant) necrosis cells; (upper right quadrant) late-apoptotic cells; (bottom left quadrant) live cells; and (bottom right quadrant) early apoptotic cells; (B) Histograms display the percentage of cell distribution after treatment with **7f**.

2.8 *In vitro* evaluation of anti-vascular activity

To evaluate the anti-vascular activity of compound **7f**, the HUVEC culture assays were performed to assess the ability of **7f** to inhibit HUVECs migration which is the key step to generate new blood vessels. As shown in Fig. 9A, the untreated cells migrated to fill the area that was initially scraped after 24 h. In contrast, compound **7f** significantly inhibited the HUVEC migration in a dose-dependent manner.

Then we further evaluated the anti-vascular activity of compound **7f** in a tube formation assay. After being seeded on Matrigel, HUVECs form the capillary-like tubules with multicentric junctions. After exposure to **7f** at 0.03, 0.06, and 0.12 μM for 6 h, the capillary-like tubes were interrupted in different levels (Fig. 9B). These results showed that compound **7f** can effectively inhibit the tube formation of HUVECs.

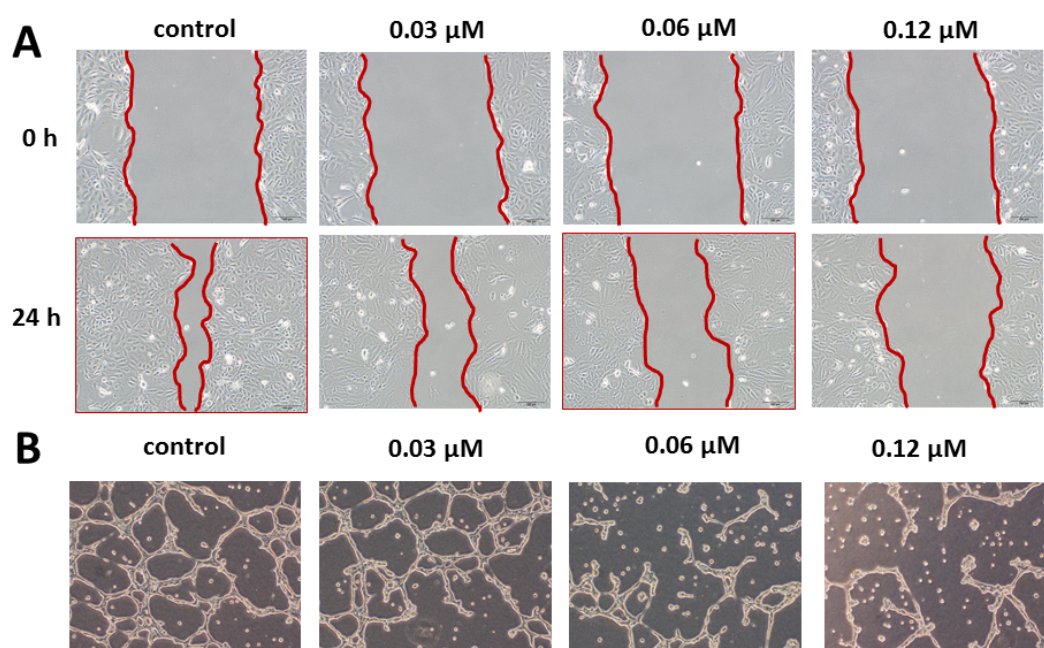


Figure 9. Effects of compound **7f** on the HUVECs migration and tube formation. (A) Scratches were created with sterile 200 μL pipette and images were captured using phase contrast

microscopy at 0 h and 24 h after treatment with 0, 0.03, 0.06, and 0.12 μM of compound **7f**. (B) Images depicting the formation of HUVEC capillary-like tubular network by treatment with 0, 0.03, 0.06, and 0.12 μM of compound **7f** for 6 h.

2.9 *In vivo* antitumor activity of **7f**

Based on the *in vitro* antiproliferative activity and mechanism studies, we further tested the *in vivo* antitumor activity of **7f**. Liver cancer xenograft mouse model was established by subcutaneous inoculation of H22 cells into the right flank of mice. The tumor size and body weights of the mice were monitored and recorded every 2 days. Paclitaxel (PTX) and CA-4 were selected as the positive control. As shown in Fig. 10A, **7f** at the dose of 30 mg/kg per day and PTX at the dose of 8 mg/kg per 2 days significantly decreased the tumor volume. The reduction in tumor weight reached 72.4% at a dose of 8 mg/kg per 2 days (i.v.) of PTX at 21 days after initiation of treatment as compared to vehicle, and **7f** reduced tumor weights by 51.6% and 63.6% at doses of 15 and 30 mg/kg per day (i.v.), respectively (Fig. 10C), which was more potent than CA-4 (inhibitory rates of 46.2% and 55.4% at doses of 15 and 30 mg/kg per day, respectively). Moreover, **7f** did not affect body weight even at the dose of 30 mg/kg, while treatment with PTX at a dose of 8 mg/kg per 2 days led to a significant decrease of body weight (Fig. 10B). Thus, compound **7f** is worthy of further investigation for the treatment of cancers.

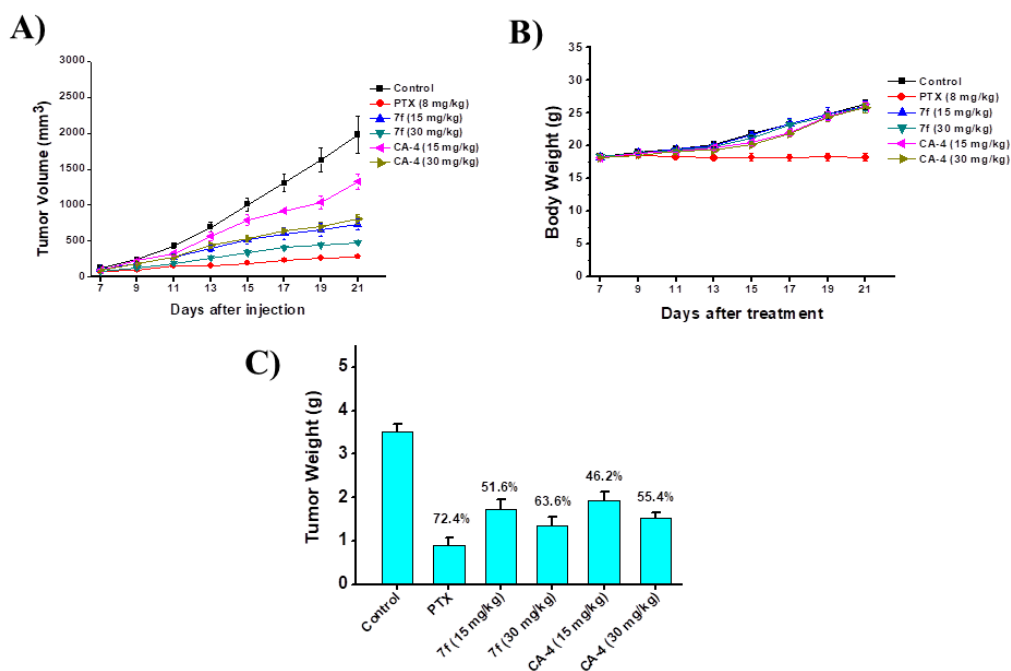


Figure 10. A) Tumor growth curves after injection with different formulations in H22 tumor bearing mice; B) Body weight changes of mice during treatment; C) **7f** treatment resulted in significantly lower tumor weight compared with controls.

2.9 Docking study

To illustrate the binding mode of the most active compound **7f** with tubulin, we performed a docking study of **7f** into the colchicine binding pocket of tubulin (PDB: 1SA0) by using the DOCK program in Discovery Studio 3.0 software. As shown in Fig. 11, **7f** and colchicine adopted a similar positioning at the colchicine binding pocket. The trimethoxyphenyl ring of **7f** was located in a hydrophobic pocket and the methoxy group at C-4 position formed hydrogen bond with the critical residue Cys 241; the indole ring extended into another hydrophobic cavity as similar to the tropone of colchicine.

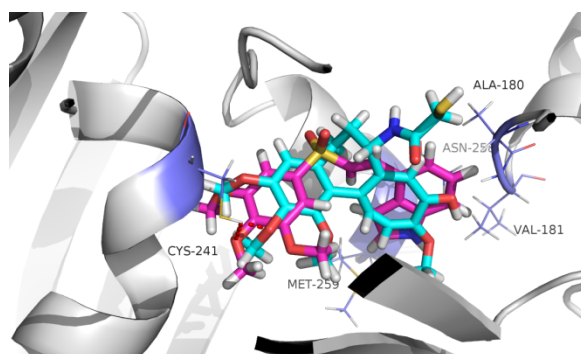


Figure 11. Proposed binding model for **7f** (magenta) binding with tubulin (PDB code: 1SA0), and overlapping with DAMA-colchicine (cyan).

3. Conclusions

In summary, a series of novel indole-vinyl sulfone derivatives were further designed, synthesized, and evaluated as tubulin polymerization inhibitors based on our previous work. Osiris calculations were performed on all target compounds to estimate their physicochemical and drug-likeness properties, and the results indicated that most compounds improved the drug-likeness properties compared to our previously compound **4**. Preliminary anti-proliferative screening of nine new compounds showed that vinyl moieties substituted at C-4 position of indole ring was favorable. Following modifications of **7f** led to the synthesis and biological evaluations of further thirteen derivatives. Among them, compound **7f** displayed the most potent activity against a panel of cancer cell lines with IC_{50} values ranging from 55 to 305 nM, which is nearly 2-7 folds more potent than compound **4**. Compound **7f** also displayed about 8-fold improvement of selective index as compared to compound **4**, indicating that **7f** might have lower toxicity. Besides, compound **7f** displayed potent inhibitory activity in tubulin polymerization assay ($IC_{50} = 3.09 \mu\text{M}$), which was slightly less potent than the positive control CA-4 ($IC_{50} = 2.17 \mu\text{M}$). Further mechanism studies demonstrated that **7f** caused cell cycle arrest at G2/M phase, induced cell apoptosis and disrupted microtubule networks in K562 cells with a dose-dependent manner. Furthermore, the wound healing and tube formation assays also identified **7f** as a novel vascular disrupting agent. Moreover, molecular modelling studies demonstrated that **7f** interacted with tubulin at the colchicine binding site. Finally, the *in vivo* anti-tumor activity of **7f** was validated in H22 liver cancer xenograft mouse model. Collectively, **7f** may represent a novel anti-tubulin agent with clinical potential for the treatment of cancers.

4. Experimental

4.1 Chemistry

4.1.1. General

Most chemicals and solvents were purchased from commercial sources. Further purification and drying by standard methods were employed when necessary. ¹H NMR and ¹³C NMR spectra were recorded on Bruker-300 spectrometers in the indicated solvents (TMS as internal standard). Data are reported as follows: chemical shift in ppm (d), multiplicity (s =singlet, d =doublet, t =triplet, q =quartet, brs = broad singlet, m =multiplet), coupling constant (Hz), and integration. High Resolution Mass measurement was performed on Agilent QTOF 6520 mass spectrometer with electron spray ionization (ESI) as the ion source. Flash column chromatography was carried out using commercially available silica gel (200-300 mesh) under pressure.

4.1.2. Synthesis of intermediates **5a-k**.

Intermediates **5a-k** were synthesized according to the procedures reported in our previous article [20].

4.1.3 General procedures of compound **7a-n**, **8a-d**.

To a solution of **5** (0.2 mmol) in anhydrous THF, NaH (60%, 0.24 mmol) was added at 0 °C under N₂ atmosphere. After stirring for 15 min, aromatic aldehyde (0.24 mmol) was added into the mixture and the reaction was stirred for another 1 h. The reaction mixture was then extracted with EtOAc (3 × 20 mL). The combined organic layers were then washed with saturated brine, dried over anhydrous Na₂SO₄, and concentrated in vacuo. The residue was purified by flash column chromatography using PE/EA (5/1, V/V) as an eluent to afford the compounds **7a-n**, **8a-d**.

4.1.3.1. Compound 7a. White solid, yield 86.7%, m.p. 157-159 °C. ¹H NMR (300 MHz, CDCl₃) δ 8.86 (s, 1H), 7.60 (d, *J* = 15.0 Hz, 1H), 7.14 (s, 2H), 7.08 (s, 1H), 6.79 (s, 1H), 6.49 (d, *J* = 15.0 Hz, 1H), 6.37 (s, 1H), 3.90 (s, 6H), 3.88 (s, 3H); ¹³C NMR (75 MHz, CDCl₃) δ 152.98, 141.33, 136.39, 136.03, 122.27, 121.03, 120.03, 118.02, 106.25, 104.15, 60.43, 55.96; HR-MS (ESI) *m/z*: calcd for C₁₅H₁₈NO₅S [M+H]⁺ 324.0900, found 324.0897.

4.1.3.2. Compound 7b. Red oil, yield 85.2%. ¹H NMR (300 MHz, CDCl₃) δ 8.67 (d, *J* = 6.0 Hz, 2H), 7.57 (d, *J* = 15.0 Hz, 1H), 7.36 (d, *J* = 6.0 Hz, 2H), 7.17 (s, 2H), 7.08 (d, *J* = 15.0 Hz, 1H), 3.93 (s, 6H), 3.92 (s, 3H); ¹³C NMR (75 MHz, CDCl₃) δ 153.73,

150.63, 142.82, 139.76, 138.63, 134.03, 132.38, 122.08, 105.26, 60.95, 56.54; HR-MS (ESI) m/z: calcd for C₁₆H₁₈NO₅S [M+H]⁺ 336.0900, found 336.0897.

4.1.3.3 Compound 7c. Yellow solid, yield 75.6%, m.p. 190-192 °C. ¹H NMR (300 MHz, DMSO-*d*₆) δ 11.77 (s, 1H), 7.97 (d, *J* = 2.7 Hz, 1H), 7.81 (d, *J* = 15.4 Hz, 1H), 7.38 (d, *J* = 8.8 Hz, 2H), 7.26 (s, 2H), 7.20 (d, *J* = 15.4 Hz, 1H), 6.88 (dd, *J* = 2.0, 9.0 Hz, 1H), 3.89 (s, 6H), 3.85 (s, 3H), 3.74 (s, 3H); ¹³C NMR (75 MHz, DMSO-*d*₆) δ 155.04, 153.08, 140.93, 137.47, 136.17, 133.29, 132.21, 125.29, 119.43, 113.08, 112.44, 109.83, 104.20, 102.42, 60.14, 56.32, 55.74; HR-MS (ESI) m/z: calcd for C₂₀H₂₂NO₆S [M+H]⁺ 404.1162, found 404.1156.

4.1.3.4 Compound 7d. Yellow solid, yield 76.0%, m.p. 188-190 °C. ¹H NMR (300 MHz, DMSO-*d*₆) δ 11.69 (s, 1H), 7.89 (s, 2H), 7.76 (d, *J* = 15.3 Hz, 1H), 7.24 (s, 2H), 7.17 (d, *J* = 15.6 Hz, 1H), 6.98 (s, 1H), 6.83 (d, *J* = 6.0 Hz, 1H), 3.89 (s, 6H), 3.80 (s, 3H), 3.74 (s, 3H); ¹³C NMR (75 MHz, DMSO-*d*₆) δ 156.35, 153.08, 140.95, 138.40, 137.28, 135.98, 132.46, 120.80, 119.71, 118.55, 110.80, 110.11, 104.22, 95.51, 60.13, 56.30, 55.19; HR-MS (ESI) m/z: calcd for C₂₀H₂₂NO₆S [M+H]⁺ 404.1162, found 404.1163.

4.1.3.5 Compound 7e. Yellow solid, yield 66.7%, m.p. 195-197 °C. ¹H NMR (300 MHz, CDCl₃) δ 9.11 (s, 1H), 7.87 (d, *J* = 15.3 Hz, 1H), 7.77 (d, *J* = 6.9 Hz, 1H), 7.55 (d, *J* = 2.9 Hz, 1H), 7.44 (dd, *J* = 6.7, 1.6 Hz, 1H), 7.30 – 7.22 (m, 2H), 7.19 (s, 2H), 6.81 (d, *J* = 15.3 Hz, 1H), 3.91 (s, 6H), 3.89 (s, 3H); ¹³C NMR (75 MHz, CDCl₃) δ 153.50, 141.71, 137.18, 136.59, 136.20, 130.63, 124.87, 123.68, 121.88, 120.98, 120.07, 112.19, 111.37, 104.53, 60.99, 56.47; HR-MS (ESI) m/z: calcd for C₁₉H₂₀NO₅S [M+H]⁺ 374.1057, found 374.1053.

4.1.3.6 Compound 7f. White solid, yield 86.6%, m.p. 172-174 °C. ¹H NMR (300 MHz, CDCl₃) δ 8.75 (s, 1H), 8.04 (d, *J* = 15.5 Hz, 1H), 7.48 (d, *J* = 7.9 Hz, 1H), 7.33 – 7.29 (m, 2H), 7.21 (s, 2H), 7.17 (t, *J* = 7.6 Hz, 1H), 7.03 (d, *J* = 16.5 Hz, 1H), 6.75 (s, 1H), 3.90 (s, 9H); ¹³C NMR (75 MHz, CDCl₃) δ 153.60, 142.19, 141.31, 136.38, 135.79, 126.96, 126.63, 126.26, 124.27, 121.87, 121.59, 114.40, 104.95, 100.90, 60.96, 56.51; HR-MS (ESI) m/z: calcd for C₁₉H₂₀NO₅S [M+H]⁺ 374.1057, found 374.1051.

4.1.3.7 Compound 7g. White solid, yield 83.2%, m.p. 203-205 °C. ¹H NMR (300

MHz, DMSO-*d*₆) δ 11.28 (s, 1H), 7.83 (s, 1H), 7.58 (d, *J* = 15.3 Hz, 1H), 7.41 – 7.32 (m, 4H), 7.10 (s, 2H), 6.40 (s, 1H), 3.78 (s, 6H), 3.64 (s, 3H); ¹³C NMR (75 MHz, DMSO-*d*₆) δ 153.65, 144.03, 141.68, 137.90, 136.87, 128.28, 127.38, 124.38, 123.98, 123.60, 121.66, 112.54, 104.78, 102.61, 60.66, 56.79; HR-MS (ESI) *m/z*: calcd for C₁₉H₂₀NO₅S [M+H]⁺ 374.1057, found 374.1055.

4.1.3.8 Compound 7h. White solid, yield 84.5%, m.p. 181-183 °C. ¹H NMR (300 MHz, CDCl₃) δ 8.70 (s, 1H), 7.79 (d, *J* = 15.3 Hz, 1H), 7.62 (d, *J* = 8.3 Hz, 1H), 7.58 (s, 1H), 7.32 (t, *J* = 2.8 Hz, 1H), 7.29-7.27 (m, 1H), 7.17 (s, 2H), 6.85 (d, *J* = 15.3 Hz, 1H), 6.57 – 6.55 (m, 1H), 3.89 (s, 9H); ¹³C NMR (75 MHz, CDCl₃) δ 153.06, 143.33, 141.47, 135.34, 135.24, 130.00, 126.74, 125.58, 123.67, 120.81, 118.91, 112.74, 104.18, 102.69, 60.49, 55.95; HR-MS (ESI) *m/z*: calcd for C₁₉H₂₀NO₅S [M+H]⁺ 374.1057, found 374.1055.

4.1.3.9 Compound 7i. White solid, yield 88.8%, m.p. 152-154 °C. ¹H NMR (300 MHz, CDCl₃) δ 9.47 (s, 1H), 8.22 (d, *J* = 15.4 Hz, 1H), 7.72 (d, *J* = 7.8 Hz, 1H), 7.38 (d, *J* = 7.4 Hz, 1H), 7.23-7.20 (m, 3H), 7.17-7.06 (m, 2H), 6.57 (dd, *J* = 3.2, 1.8 Hz, 1H), 3.88 (s, 3H), 3.85 (s, 6H); ¹³C NMR (75 MHz, CDCl₃) δ 153.67, 142.25, 139.16, 135.19, 134.48, 129.30, 125.95, 125.47, 124.61, 122.60, 119.94, 116.02, 104.71, 103.19, 61.01, 56.48; HR-MS (ESI) *m/z*: calcd for C₁₉H₂₀NO₅S [M+H]⁺ 374.1057, found 374.1052.

4.1.3.10 Compound 7j. White solid, yield 68.6%, m.p. 117-119 °C. ¹H NMR (300 MHz, CDCl₃) δ 8.57 (s, 1H), 8.21 (s, 1H), 7.45 (d, *J* = 9.7 Hz, 1H), 7.31 (s, 1H), 7.23 (d, *J* = 7.5 Hz, 1H), 7.18 (s, 2H), 7.14 (d, *J* = 7.5 Hz, 1H), 6.61 (s, 1H), 3.91 (s, 9H), 2.17 (s, 3H); ¹³C NMR (75 MHz, CDCl₃) δ 152.98, 141.47, 136.55, 135.35, 135.20, 133.44, 127.20, 125.13, 124.82, 121.22, 119.85, 111.98, 104.87, 100.49, 60.53, 55.99, 13.21; HR-MS (ESI) *m/z*: calcd for C₂₀H₂₂NO₅S [M+H]⁺ 388.1213, found 388.1209.

4.1.3.11 Compound 7k. White solid, yield 58.3%, m.p. 155-157 °C. ¹H NMR (300 MHz, CDCl₃) δ 8.57 (s, 1H), 7.55 (d, *J* = 1.47 Hz, 1H), 7.53 (d, *J* = 32.25 Hz, 1H), 7.44 (d, *J* = 4.23 Hz, 1H), 7.33 (t, *J* = 2.7 Hz, 1H), 7.25 (s, 2H), 7.21 (t, *J* = 7.9 Hz, 1H), 6.73 (s, 1H), 3.92 (s, 3H), 3.92 (s, 6H); ¹³C NMR (75 MHz, CDCl₃) δ 153.10, 152.68 (d, *J* = 301.50 Hz), 142.49, 135.42, 131.54, 127.64, 125.21, 121.64, 121.43 (d,

$J = 12$ Hz), 120.41 (d, $J = 3.75$ Hz), 113.02 (d, $J = 2.25$ Hz), 112.53, 105.32, 100.26, 60.56, 56.04; HR-MS (ESI) m/z : calcd for $C_{19}H_{19}FNO_5S$ $[M+H]^+$ 392.0962, found 392.0963.

4.1.3.12 Compound 7l. White solid, yield 48.9%, m.p. 144-146 °C. 1H NMR (300 MHz, $CDCl_3$) δ 8.60 (s, 1H), 8.51 (s, 1H), 7.91 (d, $J = 7.6$ Hz, 1H), 7.51 (d, $J = 8.1$ Hz, 1H), 7.36 (t, $J = 2.9$ Hz, 1H), 7.27 - 7.22 (m, 3H), 6.75 (ddd, $J = 3.2, 2.0, 0.9$ Hz, 1H), 3.93 (s, 3H), 3.92 (s, 6H); ^{13}C NMR (75 MHz, $CDCl_3$) δ 152.91, 142.21, 135.36, 131.99, 131.49, 129.21, 128.37, 125.34, 122.26, 121.27, 120.17, 113.61, 105.76, 100.19, 60.56, 56.04; HR-MS (ESI) m/z : calcd for $C_{19}H_{19}ClNO_5S$ $[M+H]^+$ 408.0667, found 408.0663.

4.1.3.13 Compound 7m. Colourless oil, yield 50.3%. 1H NMR (300 MHz, $CDCl_3$) δ 8.59 (s, 1H), 7.68 (s, 1H), 7.66 (d, $J = 7.3$ Hz, 1H), 7.45 (d, $J = 8.1$ Hz, 1H), 7.33 (dd, $J = 3.3, 2.5$ Hz, 1H), 7.23 (s, 2H), 7.20 (d, $J = 7.9$ Hz, 1H), 6.76 - 6.74 (m, 1H), 3.91 (s, 9H), 3.82 (s, 3H); ^{13}C NMR (75 MHz, $CDCl_3$) δ 152.91, 152.33, 141.81, 135.42, 133.18, 127.56, 124.96, 122.42, 121.64, 120.46, 119.22, 112.41, 105.12, 100.56, 61.40, 60.51, 55.98; HR-MS (ESI) m/z : calcd for $C_{20}H_{22}NO_6S$ $[M+H]^+$ 404.1162, found 404.1161.

4.1.3.14 Compound 7n. White solid, yield 85.4%, m.p. 181-183 °C. 1H NMR (300 MHz, $CDCl_3$) δ 7.67 (d, $J = 15.4$ Hz, 1H), 7.15 (s, 2H), 7.02 (t, $J = 7.8$ Hz, 1H), 6.83 (d, $J = 7.8$ Hz, 1H), 6.77 (d, $J = 15.4$ Hz, 1H), 6.65 (d, $J = 7.7$ Hz, 1H), 3.92 (s, 6H), 3.90 (s, 3H), 3.62 (t, $J = 8.5$ Hz, 2H), 3.16 (t, $J = 8.4$ Hz, 2H); ^{13}C NMR (75 MHz, $CDCl_3$) δ 153.58, 152.49, 142.14, 140.04, 135.34, 130.18, 128.74, 128.08, 127.67, 117.41, 111.24, 104.83, 61.00, 56.50, 47.03, 29.02; HR-MS (ESI) m/z : calcd for $C_{19}H_{22}NO_5S$ $[M+H]^+$ 388.1213, found 388.1205.

4.1.3.14 Compound 8a. Green oil, yield 49.3%. 1H NMR (300 MHz, $CDCl_3$) δ 9.06 (s, 1H), 7.76 (d, $J = 16.0$ Hz, 1H), 7.43 (d, $J = 8.1$ Hz, 1H), 7.29 - 7.25 (m, 2H), 7.15 (t, $J = 7.6$ Hz, 1H), 7.00 (d, $J = 16.5$ Hz, 1H), 6.96 (s, 2H), 6.72 (s, 1H), 3.87 (s, 9H); ^{13}C NMR (75 MHz, $CDCl_3$) δ 154.14, 140.20, 139.01, 136.71, 136.44, 132.57, 126.61, 125.85, 125.59, 121.79, 120.20, 113.27, 101.73, 100.72, 60.91, 56.41; HR-MS (ESI) m/z : calcd for $C_{19}H_{20}NO_4S$ $[M+H]^+$ 358.1108, found 358.1101.

4.1.3.15 Compound 8b. Colourless oil, yield 39.6%. ¹H NMR (300 MHz, CDCl₃) δ 8.89 (s, 1H), 7.81 (s, 1H), 7.42 (d, *J* = 7.7 Hz, 1H), 7.29 (t, *J* = 2.7 Hz, 1H), 7.22 – 7.13 (m, 2H), 6.94 (s, 2H), 6.61 (s, 1H), 3.89 (s, 3H), 3.88 (s, 6H), 1.96 (d, *J* = 1.4 Hz, 3H); ¹³C NMR (75 MHz, CDCl₃) δ 153.89, 142.36, 139.74, 137.75, 135.96, 131.71, 127.52, 126.41, 125.19, 121.66, 120.13, 111.93, 101.80, 100.81, 60.98, 56.36, 29.71; HR-MS (ESI) *m/z*: calcd for C₂₀H₂₂NO₄S [M+H]⁺ 372.1264, found 372.1259.

4.1.3.16 Compound 8c. Yellow solid, yield 35.5%, m.p. 80-82 °C. ¹H NMR (300 MHz, CDCl₃) δ 8.74 (s, 1H), 7.69 (s, 1H), 7.49 (d, *J* = 8.0 Hz, 1H), 7.37 – 7.32 (m, 2H), 7.28 – 7.23 (m, 1H), 6.74 (s, 2H), 6.63 - 6.61 (m, 1H), 3.86 (s, 3H), 3.77 (s, 6H); ¹³C NMR (75 MHz, CDCl₃) δ 153.27, 140.03, 136.12, 135.83, 135.38, 126.40, 125.05, 124.14, 121.39, 120.48, 119.88, 112.18, 101.00, 100.37, 60.45, 55.76; HR-MS (ESI) *m/z*: calcd for C₁₉H₁₉ClNO₄S [M+H]⁺ 392.0718, found 392.0714.

4.1.3.17 Compound 8d. Yellow solid, yield 59.5%, m.p. 108-110 °C. ¹H NMR (300 MHz, CDCl₃) δ 7.75 (d, *J* = 15.6 Hz, 1H), 7.36 (d, *J* = 7.9 Hz, 1H), 7.29 (d, *J* = 6.3 Hz, 1H), 7.23 (d, *J* = 7.7 Hz, 1H), 7.16 (d, *J* = 3.2 Hz, 1H), 7.00 (d, *J* = 15.6 Hz, 1H), 6.95 (s, 2H), 6.69 (d, *J* = 3.0 Hz, 1H), 3.90 (s, 6H), 3.88 (s, 3H), 3.82 (s, 3H); ¹³C NMR (75 MHz, CDCl₃) δ 153.59, 139.48, 138.63, 136.67, 135.77, 132.36, 129.73, 126.65, 125.30, 121.02, 119.32, 110.66, 101.02, 98.88, 60.44, 55.90, 32.59; HR-MS (ESI) *m/z*: calcd for C₂₀H₂₂NO₄S [M+H]⁺ 372.1264, found 372.1257.

4.1.4 Compound 7o. To a solution of **7f** (50 mg, 0.13 mmol) in glacial acetic acid, sodium cyanoborohydride (17 mg, 0.26 mmol) was added. After stirring for 2 h, acetic acid was removed in vacuo and the residue was then was extracted with EtOAc (3 × 20 mL). The combined organic layers were then washed with saturated brine, dried over anhydrous Na₂SO₄, and concentrated in vacuo. The residue was purified by flash column chromatography using PE/EA (5/1,V/V) as an eluent to afford the compound **7o** (30 mg, 65.5%) as grey solid, m.p. 108-110 °C. ¹H NMR (300 MHz, CDCl₃) δ 8.03 (d, *J* = 15.4 Hz, 1H), 7.41 (d, *J* = 8.0 Hz, 1H), 7.33 (d, *J* = 6.7 Hz, 1H), 7.24 (d, *J* = 7.8 Hz, 1H), 7.20 – 7.19 (m, 3H), 7.02 (d, *J* = 15.4 Hz, 1H), 6.70 (d, *J* = 3.2 Hz, 1H), 3.92 (s, 6H), 3.89 (s, 3H), 3.83 (s, 3H); ¹³C NMR (75 MHz, CDCl₃) δ 153.06, 141.50, 140.64, 136.68, 135.29, 130.25, 127.01, 126.14, 123.85, 120.97,

120.74, 111.94, 104.30, 98.92, 60.49, 55.99, 32.64; HR-MS (ESI) m/z: calcd for C₂₀H₂₂NO₅S [M+H]⁺ 376.1213, found 376.1206.

4.1.5 Compound 7p. A solution of POCl₃ (19 μL, 0.2 mmol) in DMF (1 mL) was stirred at 0 °C for 30 min, after which a solution of compound **7f** (50 mg, 0.13 mmol) in DMF was added and stirred for 2 h. Then the reaction mixture was poured onto ice with sodium acetate and stirred for 1 h. The residue was extracted with EtOAc (3 × 20 mL). The combined organic layers were then washed with saturated brine, dried over anhydrous Na₂SO₄, and concentrated in vacuo. The residue was purified by flash column chromatography using PE/EA (1/1, V/V) as an eluent to afford the compound **7p** (40 mg, 74.3%) as white solid, m.p. 210-212 °C. ¹H NMR (300 MHz, DMSO-*d*₆) δ 12.55 (s, 1H), 9.83 (s, 1H), 9.32 (d, *J* = 15.4 Hz, 1H), 8.52 (s, 1H), 7.68 (d, *J* = 7.6 Hz, 1H), 7.62 (d, *J* = 8.0 Hz, 1H), 7.46 (d, *J* = 15.4 Hz, 1H), 7.35 (d, *J* = 7.8 Hz, 1H), 7.28 (s, 2H), 3.87 (s, 6H), 3.72 (s, 3H); ¹³C NMR (75 MHz, DMSO-*d*₆) δ 184.11, 153.12, 143.83, 143.60, 141.18, 138.71, 136.23, 127.68, 126.14, 123.85, 123.30, 121.09, 119.08, 115.21, 104.40, 60.14, 56.19; HR-MS (ESI) m/z: calcd for C₂₀H₂₀NO₆S [M+H]⁺ 402.1006, found 402.1003.

4.1.6 General procedures of compound 7q, 8e.

Indole-4-aldehyde (0.33 mmol) was added to a solution of **5j** or **5k** (0.3 mmol) in toluene, after which piperidine (cat, 5 μL) and AcOH (cat, 5 μL) was then added. The mixture was refluxed and monitored by TLC. After reaction completed, toluene was removed in vacuo and the residue was extracted with EtOAc (3 × 50 mL). The combined organic layers were then washed with brine, dried over anhydrous Na₂SO₄, and concentrated in vacuo. The residue was purified by flash column chromatography using PE/EA (3/1, V/V) as an eluent to afford the compound **7q** or **8e**.

4.1.6.1 Compound 7q. Yellow solid, yield 86.3%, m.p. 164-166 °C. ¹H NMR (300 MHz, CDCl₃) δ 8.70 (s, 1H), 8.58 (s, 1H), 8.04 (d, *J* = 7.7 Hz, 1H), 7.56 (d, *J* = 8.1 Hz, 1H), 7.37 (d, *J* = 2.8 Hz, 1H), 7.19 (d, *J* = 1.3 Hz, 1H), 7.17 (s, 2H), 6.74 (s, 1H), 3.85 (s, 9H); ¹³C NMR (75 MHz, CDCl₃) δ 153.17, 147.80, 142.56, 135.66, 132.09, 129.59, 126.89, 121.74, 121.05, 120.65, 116.85, 113.67, 112.10, 105.30, 99.92, 60.59, 56.09; HR-MS (ESI) m/z: calcd for C₂₀H₁₉N₂O₅S [M+H]⁺ 399.1009, found 399.1000.

4.1.6.2 Compound 8e. Yellow solid, yield 38.3%, m.p. 169-171 °C. ¹H NMR (300 MHz, CDCl₃) δ 8.85 (s, 1H), 8.34 (s, 1H), 8.03 (d, *J* = 7.7 Hz, 1H), 7.57 (d, *J* = 8.2 Hz, 1H), 7.40 (t, *J* = 2.9 Hz, 1H), 7.28 – 7.23 (m, 1H), 7.02 (s, 2H), 6.82 (s, 1H), 3.90 (s, 9H); ¹³C NMR (75 MHz, CDCl₃) δ 154.17, 142.80, 136.27, 136.22, 129.09, 126.74, 122.81, 122.14, 120.37, 116.40, 115.85, 113.98, 101.80, 101.34, 100.34, 61.02, 56.47; HR-MS (ESI) *m/z*: calcd for C₂₀H₁₉N₂O₄S [M+H]⁺ 383.1060, found 383.1054.

4.2 Pharmacology

4.2.1 *In vitro anti-proliferative assay*

K562, HepG2 and A549 cells were purchased from Nanjing KeyGen Biotech Co. Ltd. (Nanjing, China). The cytotoxicity of the test compounds was determined using the MTT assay. Briefly, the cell lines were incubated at 37 °C in a humidified 5% CO₂ incubator for 24 h in 96-microwell plates. After medium removal, 100 μL of culture medium with 0.1% DMSO containing the test compounds at different concentrations was added to each well and incubated at 37 °C for another 72 h. The MTT (5 mg/mL in PBS) was added and incubated for another 4 h, the optical density was detected with a microplate reader at 490 nm. The IC₅₀ values were calculated according to the dose-dependent curves. All the experiments were repeated in at least three independent experiments.

4.2.2 *In vitro tubulin polymerization inhibitory assay*

An amount of 2 mg/mL tubulin (Cytoskeleton) was resuspended in PEM buffer containing 80 mM piperazine-N,N'-bis(2-ethanesulfonic acid) sequisodium salt PIPES (pH 6.9), 0.5 mM EGTA, 2 mM MgCl₂, and 15% glycerol. Then the mixture was preincubated with compounds or vehicle DMSO on ice. PEG containing GTP was added to the final concentration of 3 mg/mL before detecting the tubulin polymerization reaction. After 30 min, the absorbance of different concentrations was detected by a spectrophotometer at 340 nm at 37 °C. The area under the curve was used to determine the concentration that inhibited tubulin polymerization by 50% (IC₅₀), which was calculated with GraphPad Prism Software version 5.02.

4.2.3 *Immunofluorescence Staining*

K562 cells were seeded into 6-well plates and then treated with vehicle control

0.1% DMSO, **7f** (0, 0.03, 0.06, 0.12 μM). The cells were fixed with 4% paraformaldehyde and then penetrated with PBS for three times. After blocking for 20 min by adding 50-100 μL goat serum albumin at room temperature, cells were incubated with a monoclonal antibody (anti- α -tubulin) at 37 °C for 2 h. Then the cells were washed three times by PBS following staining by fluorescence antibody and labeling of nuclei by 4,6-diamidino-2-phenylindole (DAPI). Cells were finally visualized using a fluorescence microscope (OLYMPUS, Japan).

4.2.4 Cell cycle analysis

K562 cells were seeded into 6-well plates and incubated at 37 °C in a humidified 5% CO₂ incubator for 24 h, and then treated with or without **7f** at indicated concentrations for another 72 h. The collected cells were fixed by adding 70% ethanol at 4 °C for 12 h. Subsequently, the cells were resuspended in PBS containing 100 mL RNase A and 400 mL of propidium iodide for 30 min. The DNA content of the cells was measured using a FACS Calibur flow cytometer (Bectone Dickinson, San Jose, CA, USA).

4.2.5 Cell apoptosis analysis

After treatment with or without **7f** at indicated concentrations for 72 h, the cells were washed twice in PBS, centrifuged and resuspended in 500 mL AnnexinV binding buffer. The cells were then harvested, washed and stained with 5 mL Annexin V-APC and 5 mL 7-AAD in the darkness for 15 min. Apoptosis was analyzed using a FACS Calibur flow cytometer (Bectone Dickinson, San Jose, CA, USA).

4.2.6 Wound healing assay

K562 cells were grown in 6-well plates for 24 h. Scratches were made in confluent monolayers using 200 μL pipette tip. Then, wounds were washed twice with PBS to remove non-adherent cell debris. The media containing different concentrations (0, 0.03, 0.06, 0.12 μM) of the compound **7f** were added to the petridishes. Cells which migrated across the wound area were photographed using phase contrast microscopy at 0 h and 24 h. The migration distance of cells migrated in to the wound area was measured manually.

4.2.7 Tube formation assay

EC Matrigel matrix was thawed at 4 °C overnight, and HUVECs suspended in DMEM were seeded in 96-well culture plates at a cell density of 50,000 cells/well after polymerization of the Matrigel at 37 °C for 30 min. They were then treated with 20 μ L different concentrations of compound **7f** or vehicle for 6 h at 37 °C. Then, the morphological changes of the cells and tubes formed were observed and photographed under inverted microscope (OLYMPUS, Japan).

4.2.8 *In vivo anti-tumor evaluation*

Five-week-old male Institute of Cancer Research (ICR) mice were purchased from Shanghai SLAC Laboratory Animals Co. Ltd. A total of 1×10^6 H22 cells were subcutaneously inoculated into the right flank of ICR mice according to protocols of tumor transplant research, to initiate tumor growth. After incubation for one day, mice were weighted and at random divided into four groups of six animals. The groups treated with **7f** were administered 15, 30 mg/kg in a vehicle of 10% DMF/2% Tween 80/88% saline, respectively. The positive control group was treated with PTX (8 mg/kg) every 2 days by intravenous injection. The negative control group received 0.9% normal saline through intravenous injection. Treatments of **7f** were done at a frequency of intravenous injection one dose per day for a total 21 consecutive days while the positive group was treated with PTX one dose per two days. The mice were sacrificed after the treatments and the tumors were excised and weighed. The inhibition rate was calculated as follows: Tumor inhibitory ratio (%) = (1-average tumor weight of treated group/average tumor weight of control group) \times 100%.

4.3 *Molecular modeling*

In our study, the X-ray structure of the DAMA-colchicine- α,β -tubulin complex was downloaded from the Protein Data Bank (PDB code: 1SA0). The protein was prepared by removal of the stathmin-like domain, subunits C and D, water molecules and colchicine using Discovery Studio modules. The docking procedure was performed by employing DOCK program in Discovery Studio 3.0 software, and the structural image was obtained using PyMOL software.

Acknowledgments

The authors acknowledge the National Natural Science Foundation of China (No. 81673306, 81703348), The Open Project of State Key Laboratory of Natural Medicines, China Pharmaceutical University (No. SKLNMKF 201710), "Double First-Class" University project CPU2018GY04, China Pharmaceutical University.

Reference

1. K. Downing, E. Nogales, Tubulin structure: insights into microtubule properties and functions, *Curr. Opin. Chem. Biol.* 8 (1998) 785-791.
2. M. Jordan, L. Wilson, Microtubules as a target for anticancer drugs, *Nat. Rev. Cancer* 4 (2004) 253-265.
3. H. Kueh, T. Mitchison, Structural plasticity in actin and tubulin polymer dynamics, *Science* 325 (2009) 960-963.
4. C. Dumontet, M. Jordan, Microtubule-binding agents: a dynamic field of cancer therapeutics, *Nat. Rev. Drug Discov.* 9 (2010) 790-803.
5. G. R. Pettit, S. B. Singh, E. Hamel, C. M. Lin, D. S. Alberts, D. Garcia-Kendal, Isolation and structure of the strong cell growth and tubulin inhibitor combretastatin A-4, *Experientia.* 45 (1989) 209-211.
6. G. R. Pettit, J. C. Temple, V. L. Narayanan, R. Varma, M. J. Simpson, M. R. Boyd, N. Bansal, Antineoplastic agents 322. Synthesis of combretastatin A-4 prodrugs, *Anti-Cancer Drug Des.* 10 (1995) 299-309.
7. C. Stengel, S. P. Newman, M. P. Leese, B. V. Potter, M. J. Reed, A. Purohit, Class III beta-tubulin expression and in vitro resistance to microtubule targeting agents, *Br. J. Cancer.* 102 (2010) 316-324.
8. Y. Lu, J. J. Chen, M. Xiao, W. Li, D. D. Miller, An overview of tubulin inhibitors that interact with the colchicine binding site, *Pharm. Res.* 29 (2012) 2943-2971.
9. E. Porcù, R. Bortolozzi, G. Basso, G. Viola, Recent advances in vascular disrupting agents in cancer therapy, *Future Med. Chem.* 6 (2014) 1485-1498.
10. M. J. Perez-Perez, E. M. Priego, O. Bueno, M. S. Martins, M. D. Canela, S. Liekens, Blocking blood flow to solid tumors by destabilizing tubulin: An approach to

- targeting tumor growth, *J. Med. Chem.* 59 (2016) 8685-8711.
11. Y. Y. Leung, L. L. Hui, V. B. Kraus, Colchicine-Update on mechanisms of action and therapeutic uses, *Seminars in Arthritis and Rheumatism*, 45 (2015) 341-350.
 12. G. R. Pettit, S. B Singh, M. R. Boyd, E. Hamel, R. K. Perrit, J. M. Schmidt, F. Hogan, Antineoplastic agents. 291. Isolation and synthesis of combretastatins A-4, A-5, and A-6, *J. Med. Chem.* 38 (1995) 1666-1672.
 13. L. Lee, R. Davis, J. Vanderham, P. Hills, H. Mackay, T. Brown, S. L. Mooberry, M. Leea, 1, 2, 3, 4-Tetrahydro-2-thioxopyrimidine analogs of combretastatin-A4, *Eur. J. Med. Chem.* 43 (2008) 2011-2015.
 14. M. Driowya, J. Leclercq, V. Verones, A. Barczyk, M. Lecoeur, N. Renault, N. Flouquet, A. Ghinet, P. Berthelot, N. Lebegue, Synthesis of triazoloquinazolinone based compounds as tubulin polymerization inhibitors and vascular disrupting agents, *Eur. J. Med. Chem.* 115 (2016) 393-405.
 15. M. Mustafa, D. Abdelhamid, E. M. N. Abdelhafez, M. A. A. Ibrahim, A. M. Gamal-Eldeen, O. M. Aly, Synthesis, antiproliferative, anti-tubulin activity, and docking study of new 1,2,4-triazoles as potential combretastatin analogues, *Eur. J. Med. Chem.* 141 (2017) 293-305.
 16. R. Kaur, G. Kaur, R. K. Gill, R. Soni, J. Bariwal, Recent developments in tubulin polymerization inhibitors: An overview, *Eur. J. Med. Chem.* 87 (2014) 89-124.
 17. W. Li, H. Sun, S. Sun, Z. Zhu, J. Xu, Tubulin inhibitors targeting the colchicine binding site: a perspective of privileged structures, *Future med. chem.* 9 (2017) 1765-1794.
 18. S. A. Patil, R. Patil, D. D. Miller, Indole molecules as inhibitors of tubulin polymerization: potential new anticancer agents, *Future Med. Chem.* 4 (2012) 2085-2115.
 19. R. Patil, S. A. Patil, K. D. Beaman, S. A. Patil, Indole molecules as inhibitors of tubulin polymerization: potential new anticancer agents, an update (2013-2015), *Future Med. Chem.* 8 (2016) 1291-1316.
 20. W. Li, Y. Yin, H. Yao, W. Shuai, H. Sun, S. Xu, J. Liu, H. Yao, Z. Zhu, J. Xu, Discovery of novel vinyl sulfone derivatives as anti-tumor agents with microtubule

polymerization inhibitory and vascular disrupting activities. *Eur. J. Med. Chem.* 157 (2018) 1068-1080.

21. W. Li, W. Shuai, F. Xu, H. Sun, S. Xu, H. Yao, J. Liu, H. Yao, Z. Zhu, J. Xu, Discovery of novel 4-arylisochromenes as anticancer agents with inhibitory activity of tubulin polymerization. *ACS Med. Chem. Lett.* 9 (2018) 974-979.

22. W. Li, Y. Yin, W. Shuai, F. Xu, H. Yao, J. Liu, K. Cheng, J. Xu, Z. Zhu, S. Xu. Discovery of novel quinazolines as potential anti-tubulin agents occupying three zones of colchicine domain. *Bioorg. Chem.* 83 (2019) 380-390.

23. A. S. Kalgutka, I. Gardner, R. S. Obach, C. L. Shaffe, E. Callegar, K. R. Henne, A. E. Mutlib, D. K. Dalvie, J. S. Lee, Y. Nakai, J. P. O'Donnell, J. Boer, S. P. Harriman, A comprehensive listing of bioactivation pathways of organic functional groups, *Curr. Drug Metab.* 6 (2005) 161-225.

24. M.L. Crismon, Tacrine: first drug approved for Alzheimer's disease, *Ann. Pharmacother.* 28 (1994) 744-751.

25. P. B. Watkins, H. J. Zimmerman, M. J. Knapp, S. I. Gracon, K. W. Lewis, Hepatotoxic effects of tacrine administration in patients with Alzheimer's disease, *JAMA*, 271 (1994) 992-998.

26. J. Yan, J. Chen, S. Zhang, J. Hu, L. Huang, X. Li, Synthesis, evaluation, and mechanism study of novel indole-chalcone derivatives exerting effective antitumor activity through microtubule destabilization in vitro and in vivo, *J. Med. Chem.* 59 (2016) 5264-5283.

27. J. Liou, C. Wu, H. Hsieh, C. Chang, C. Chen, C. Kuo, J. Chang, 4- and 5-aryloxyindoles as novel classes of potent antitubulin agents, *J. Med. Chem.* 50 (2007) 4548-4552.

28. G. Vistoli, A. Pedretti, B. Testa, Assessing drug-likeness - what are we missing? *Drug. Discov. Today*, 13 (2008) 285-294.

29. I. Muegge, Selection criteria for drug-like compounds, *Med. Res. Rev.* 23 (2003) 302-321.

30. Shultz MD. Improving the plausibility of success with inefficient metrics, *ACS Med. Chem. Lett.* 5 (2014) 2-5.

31. A. Tarcsey, K. Nyíri, G.M. Keseru, Impact of lipophilic efficiency on compound quality, *J. Med. Chem.* 55 (2012) 1252-1260.
32. P. Ertl, B. Rodhe, P. Selzer, Fast calculation of molecular polar surface areas as a sum of fragment based contribution and its application to the prediction of drug transport properties, *J. Med. Chem.* 43 (2000) 3714-3717.
33. A. M. Alafeefy, S. I. Alqasoumi, A. E. Ashour, V. Masand, N. A. AlJaber, T. B. Hadda, M. A. Mohamed, Quinazoline-tyrphostin as a new class of antitumor agents, molecular properties prediction, synthesis and biological testing, *Eur. J. Med. Chem.* 53 (2012) 133-140.